

Low temperature specific heat and possible gap to magnetic excitations in the Heisenberg pyrochlore antiferromagnet $\text{Gd}_2\text{Sn}_2\text{O}_7$

Adrian Del Maestro¹ and Michel J. P. Gingras^{2,3}

¹*Department of Physics, Harvard University, Cambridge, Massachusetts, 02138, USA*

²*Department of Physics and Astronomy, University of Waterloo, Waterloo, Ontario, N2L 3G1, Canada*

³*Department of Physics and Astronomy, University of Canterbury, Private Bag 4800, Christchurch, New Zealand*

(Dated: August 6, 2018)

The $\text{Gd}_2\text{Sn}_2\text{O}_7$ pyrochlore Heisenberg antiferromagnet displays a phase transition to a four sub-lattice Néel ordered state at a critical temperature $T_c \sim 1$ K. The low-temperature state found via neutron scattering corresponds to that predicted by a classical model that considers nearest-neighbor antiferromagnetic exchange and long-range dipolar interactions. Despite the seemingly conventional nature of the ordered state, the specific heat C_v has been found to be described in the temperature range 350 mK $\leq T \leq 800$ mK by an anomalous power law, $C_v \sim T^2$. A similar temperature dependence of C_v has also been reported for $\text{Gd}_2\text{Ti}_2\text{O}_7$, another pyrochlore Heisenberg material. Such behavior is to be contrasted with the typical T^3 behavior expected for a three-dimensional antiferromagnet with conventional long-range order which is then generally accompanied by an $\exp(-\Delta/T)$ behavior at lower temperature where anisotropy effects induce a gap Δ to collective spin excitations. Such anomalous T^2 behavior in C_v has been argued to be correlated to an unusual energy-dependence of the density of states which also seemingly manifests itself in low-temperature spin fluctuations found in muon spin relaxation experiments. In this paper, we report calculations of C_v that consider spin wave like excitations out of the Néel order observed in $\text{Gd}_2\text{Sn}_2\text{O}_7$ via neutron scattering. We argue that the parametric $C_v \propto T^2$ does not reflect the true low-energy excitations of $\text{Gd}_2\text{Sn}_2\text{O}_7$. Rather, we find that the low-energy excitations of this material are antiferromagnetic magnons gapped by single-ion and dipolar anisotropy effects, and that the lowest temperature of 350 mK considered in previous specific heat measurements accidentally happens to coincide with a crossover temperature *below* which magnons become thermally activated and C_v takes an exponential form. We argue that further specific heat measurements that extend down to at least 100 mK are required in order to ascribe an unconventional description of magnetic excitations out of the ground state of $\text{Gd}_2\text{Sn}_2\text{O}_7$ or to invalidate the standard picture of gapped excitations proposed herein.

I. INTRODUCTION

A. Persistent spin dynamics in pyrochlores

A magnetic system with Heisenberg spins that sit on the vertices of a three-dimensional pyrochlore lattice of corner sharing tetrahedra and interact among themselves via nearest-neighbor antiferromagnetic exchange interactions is highly geometrically frustrated^{1,2,3}. Such a system is theoretically predicted to not develop conventional magnetic long range order at finite temperature for either classical^{3,4} or quantum spins⁵. As a result of this frustration, real magnetic materials with antiferromagnetically coupled spins on this pyrochlore structure are highly sensitive to weak perturbative interactions beyond nearest-neighbor exchange which dramatically affect the nature of the low temperature state. It is partially for this reason that the insulating $\text{R}_2\text{M}_2\text{O}_7$ magnetic pyrochlore oxides have attracted such a great deal of attention in recent years⁶. Indeed, this family of materials has been found to display a variety of magnetic states and exotic low temperature behaviors that strongly depend on the specific elements R and M considered⁶.

In $\text{R}_2\text{M}_2\text{O}_7$, the R site is occupied by a trivalent ion, such as diamagnetic Y^{3+} or a magnetic rare earth ion ($\text{R}=\text{Gd}^{3+}, \text{Tb}^{3+}, \text{Dy}^{3+}, \text{Ho}^{3+}, \text{Er}^{3+}, \text{Tm}^{3+}, \text{Yb}^{3+}$) while

the M site is occupied by a tetravalent ion which can be diamagnetic, such as Ti^{4+} or Sn^{4+} , or magnetic, such as Mo^{4+} or Mn^{4+} . Both the R and M sites form distinct interpenetrating lattices of corner-shared tetrahedra and either site can be magnetic or non-magnetic^{1,6}. Such freedom allows for a large variety of phenomenology in the pyrochlore materials. This includes spin glasses like $\text{Y}_2\text{Mo}_2\text{O}_7$ ^{7,8,9,10} and $\text{Tb}_2\text{Mo}_2\text{O}_7$ ¹¹, spin ices such as $\text{Ho}_2\text{Ti}_2\text{O}_7$ ^{12,13,14} and $\text{Dy}_2\text{Ti}_2\text{O}_7$ ¹⁵, conventional long range ordered materials like $\text{Gd}_2\text{Ti}_2\text{O}_7$ ^{16,17,18,19} and $\text{Gd}_2\text{Sn}_2\text{O}_7$ ²⁰ and even possible spin liquids as in the case of $\text{Tb}_2\text{Ti}_2\text{O}_7$ ^{21,22,23,24,25,26}.

One common thread throughout these various materials is that several experimental studies have found that, almost without exceptions^{27,28}, *all* insulating rare-earth pyrochlore materials $\text{R}_2\text{Ti}_2\text{O}_7$ and $\text{R}_2\text{Sn}_2\text{O}_7$ display temperature-independent spin dynamics down to $T_0 \sim \mathcal{O}(10^1)$ mK. Indeed, residual low temperature dynamics has been found in pyrochlore magnetic materials with low temperature states that range from not understood whatsoever^{21,29} to seemingly conventional long range ordered^{16,17,18,19,20}. We note in passing that persistent low-temperature spin dynamics has also been found in the $\text{Gd}_3\text{Ga}_5\text{O}_{12}$ garnet (GGG)^{30,31} and in the $\text{SrCr}_8\text{Ga}_4\text{O}_{19}$ kagome antiferromagnet³². We now briefly review the various experimentally observed behaviors of the $\text{R}_2\text{Ti}_2\text{O}_7$ and $\text{R}_2\text{Sn}_2\text{O}_7$ pyrochlore oxides.

Strong evidence for fluctuating spins down to extremely low temperatures has been observed in $\text{Tb}_2\text{Ti}_2\text{O}_7$ where Ti^{4+} at the M site is non-magnetic²¹. The reason for the failure of $\text{Tb}_2\text{Ti}_2\text{O}_7$ to develop long-range magnetic order above 50 mK²² despite a Curie-Weiss temperature, $\theta_{\text{CW}} \sim -14$ K remains to this day largely unexplained^{24,25,26}. $\text{Yb}_2\text{Ti}_2\text{O}_7$ is perhaps just as intriguing, with specific heat measurements revealing a sharp first order transition at $T_c \approx 0.24$ K^{29,33}, but with the spins not appearing static below T_c since muon spin relaxation (μSR) and Mössbauer spectroscopy finds significant spin dynamics down to the lowest temperature²⁹. Hence, the observed first order transition in $\text{Yb}_2\text{Ti}_2\text{O}_7$ seems rather unconventional.

$\text{Ho}_2\text{Ti}_2\text{O}_7$ ^{12,13,14} and $\text{Dy}_2\text{Ti}_2\text{O}_7$ ¹⁵ are frustrated ferromagnets¹² and possess an extensive low-temperature magnetic entropy^{14,15} similar to that of the common hexagonal I_h phase of water ice^{34,35}. As such, the $(\text{Ho},\text{Dy})_2(\text{Ti},\text{Sn})_2\text{O}_7$ materials are referred to as *spin ices*³⁶. Theoretical and numerical studies have shown that the spin ice behavior originates from the long range nature of magnetic dipole-dipole interactions^{36,37}. Numerical Monte Carlo studies using non-local loop dynamics predict that those interactions should lead to long range order at low temperatures³⁸. Yet, at variance with the numerical predictions, experimental studies of the $\text{Dy}_2\text{Ti}_2\text{O}_7$ ³⁹ and $\text{Ho}_2\text{Ti}_2\text{O}_7$ ^{12,40,41} have not found a transition to long range order down to 60 mK. In particular, muon spin relaxation (μSR)⁴⁰ and neutron spin echo⁴¹ experiments find evidence for Ho^{3+} spin dynamics well below T_{SI} in $\text{Ho}_2\text{Ti}_2\text{O}_7$. Interestingly, a recent neutron scattering study on $\text{Tb}_2\text{Sn}_2\text{O}_7$ found a transition to a long-range ordered state at $T_c \approx 0.87$ K, with an analysis of the scattering intensity indicating that the observed state is a long-range spin ice state⁴². However, even more recent μSR studies find that the state at $T < T_c$ in $\text{Tb}_2\text{Sn}_2\text{O}_7$ remains dynamic down to the lowest temperature^{43,44}. $\text{Er}_2\text{Ti}_2\text{O}_7$, like $\text{Tb}_2\text{Sn}_2\text{O}_7$, was found via neutron scattering to display long range order below 1.2 K¹⁹. Yet, μSR found persistent spin dynamics down to the lowest temperature⁴⁵.

$\text{Gd}_2\text{Ti}_2\text{O}_7$ displays two consecutive transitions at $T_c^+ \sim 1$ K and $T_c^- \sim 0.7$ K^{16,17}. Neutron scattering experiments¹⁸ found that the magnetic state between T_c^- and T_c^+ has one site out of four on a tetrahedral unit cell that is paramagnetic and fluctuating. At $T < T_c^-$, the fourth site orders, but remains much more dynamic than the three other sites. The microscopic mechanism giving rise to the two experimentally observed states is still not understood. Here too, in $\text{Gd}_2\text{Ti}_2\text{O}_7$, μSR finds considerable spin dynamics persisting down to 20 mK^{46,47}. A phenomenological model for the density of states, $g(\epsilon)$, has been proposed for the low-temperature state of $\text{Gd}_2\text{Ti}_2\text{O}_7$. Most significantly, the proposed model for $g(\epsilon)$ was shown to describe the peculiar temperature dependence of the magnetic specific heat, $C_v(T)$, in $\text{Gd}_2\text{Ti}_2\text{O}_7$ which was found to be $C_v(T) \propto T^2$ below T_c^- . Such $C_v \propto T^2$ behavior is rather unconventional. Indeed,

in a conventional long-range ordered three-dimensional antiferromagnet, $C_v \sim T^3$ down to a temperature where the temperature dependence turns to $C_v \sim \exp(-\Delta/T)$ because of a gap Δ in the excitation spectrum induced by single ion anisotropy or anisotropic spin-spin interactions.

In all the pyrochlore systems reviewed above, $\text{Tb}_2\text{Ti}_2\text{O}_7$, $\text{Yb}_2\text{Ti}_2\text{O}_7$, $(\text{Ho},\text{Dy})_2\text{Ti}_2\text{O}_7$, $\text{Tb}_2\text{Sn}_2\text{O}_7$, $\text{Er}_2\text{Ti}_2\text{O}_7$, and $\text{Gd}_2\text{Ti}_2\text{O}_7$, some theoretical lapses exist in our understanding of the *equilibrium* thermodynamic low-temperature state. Hence, it is perhaps not completely surprising that the spin dynamics appears unconventional in these materials with, in particular, a temperature independent μSR spin polarization relaxation rate down to a baseline temperature $T_0 \sim 10^1$ mK. However, that tentative self-reassured standpoint is put on shaky ground by the μSR and specific heat measurements on $\text{Gd}_2\text{Sn}_2\text{O}_7$ that we now discuss.

B. The case of $\text{Gd}_2\text{Sn}_2\text{O}_7$

It was first proposed that the aforementioned $\text{Gd}_2\text{Ti}_2\text{O}_7$ material would be a good candidate for a classical Heisenberg pyrochlore antiferromagnet with leading perturbations coming from long-range magnetic dipole-dipole interactions¹⁶. The reason for this is that Gd^{3+} is an S-state ion with half-filled 4f shell, hence orbital angular moment $L = 0$, and spin $S = 7/2$. Spin anisotropy is therefore expected to be much smaller than for the above Ho, Dy and Tb based rare earth materials⁴⁸. In that context, $\text{Gd}_2\text{Sn}_2\text{O}_7$ should be similar to $\text{Gd}_2\text{Ti}_2\text{O}_7$; the main difference being that $\text{Gd}_2\text{Sn}_2\text{O}_7$ displays only one phase transition observed from a paramagnetic to a long-range ordered phase at $T_c \sim 1$ K²⁰. Perhaps most interestingly, unlike $\text{Gd}_2\text{Ti}_2\text{O}_7$, the experimentally observed long-range ordered phase in $\text{Gd}_2\text{Sn}_2\text{O}_7$ corresponds to the one predicted by Palmer and Chalker for the classical Heisenberg pyrochlore antiferromagnet model with perturbative long-range dipolar interactions⁴⁹. It is possible that the experimentally observed transition in $\text{Gd}_2\text{Sn}_2\text{O}_7$ corresponds to two very close transitions^{50,51} that are not resolved⁵².

From our perspective, $\text{Gd}_2\text{Sn}_2\text{O}_7$ is an exemplar of the intriguing behavior discussed above. Yet, it offers itself as a crucial system to understand. The reasons are as follows: (i) as in $\text{Gd}_2\text{Ti}_2\text{O}_7$, and all the materials previously described, persistent low-temperature spin dynamics have been observed⁵³ and (ii) again similarly to $\text{Gd}_2\text{Ti}_2\text{O}_7$, unconventional power-law temperature dependence of the magnetic specific heat has been found, specifically, $C_v \sim T^2$. So here too, there may exist the possibility to relate a dynamical response and a bulk thermodynamic measurements to an unconventional density of states $g(\epsilon)$ – a possible manifestation of the spectral down-shift that corresponds to the hallmark of highly frustrated systems. We see the experimental results on $\text{Gd}_2\text{Sn}_2\text{O}_7$ as a crucial paradox to contend

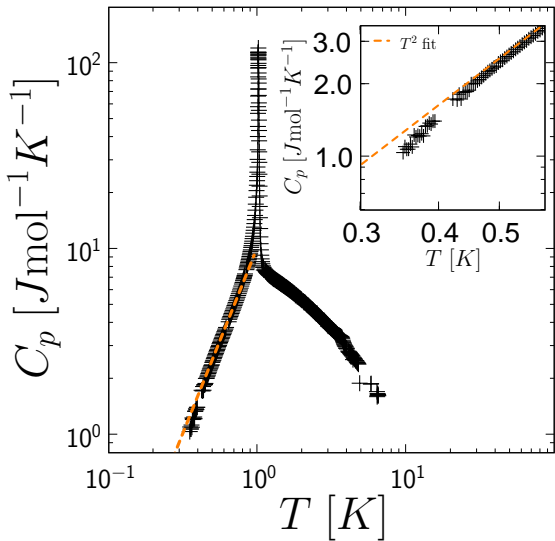


FIG. 1: (Color online) The specific heat of $\text{Gd}_2\text{Sn}_2\text{O}_7$ as a function of temperature, with an inset showing an enlargement of the low temperature region from Bonville *et al.*²⁷ plotted on a logarithmic scale. The dashed line shows the result of a relatively successful T^2 fit below 0.75 K. [Data were generously provided by P. Bonville].

with. Since the observed ordered state in $\text{Gd}_2\text{Sn}_2\text{O}_7$ corresponds to the one predicted by the model of Palmer and Chalker⁴⁹, or a more refined model that includes Gd^{3+} single-ion anisotropy^{20,54} and exchange interactions beyond nearest-neighbor^{20,50,51}, one could in principle follow the well-trodden road of solid state physics and conventional magnetism: with the Hamiltonian and consequential ground state known, identify the long wavelength excitations and, by second-quantizing them, calculate the low-temperature thermodynamic quantities. It turns out that this program was carried out in a prior work⁵⁵ for a quantum version of a simple pyrochlore lattice model with nearest-neighbor antiferromagnetic exchange plus long-range dipolar interactions^{16,49}. What was found in Ref. [55] is that *all* spin wave excitations of the Heisenberg pyrochlore antiferromagnet are pushed up in energy by the dipolar interactions and, as a result, all thermodynamic quantities show exponential temperature dependence, $\sim \exp(-\Delta/T)$, at low temperatures⁵⁵. The following question thus arises:

Do the $C_v \sim T^2$ results of Ref. [27] for $\text{Gd}_2\text{Sn}_2\text{O}_7$ contradict the theoretical prediction of Ref. [55], and are the magnetic excitations of $\text{Gd}_2\text{Sn}_2\text{O}_7$ truly unconventional?

This is the question that we ask, and aim to answer in this paper.

To spell out the question above more specifically, we show in Fig. 1 the specific heat data on $\text{Gd}_2\text{Sn}_2\text{O}_7$ reproduced from Ref. [27]. The T^2 behavior (dashed line in main panel) ranges from $T_{\text{low}} \sim 0.5$ K to $T_{\text{up}} \sim 0.8$ K. The T_{up} is very close to the critical temperature, and one

does not expect on general grounds (non-critical) power-law behaviors reflecting excitations out of the ground state to extend so close to the phase transition. Secondly, the temperature T_{low} , when compared with the results of Ref. [55], is *high* compared to the temperature regime where we expect second-quantized (spin wave) excitations to describe this system. Finally, and this is the key aspect of the data that prompted the present work, we note that the C_v data at $T \lesssim 0.5$ K progressively droop below the dashed $C_v \sim T^2$ behavior. This is emphasized in the inset of Fig. 1. Incidentally, we note from this plot that the $C_v \sim T^2$ behavior does not provide a particularly good fit of the data for $T \in [350, 800]$ mK. The crux of the argument presented in this paper is that (i) the T^2 power law between T_{low} and T_{up} is not a reflection of the low-energy properties of Gd -based antiferromagnetic pyrochlores and, most importantly, (ii) the behavior exhibited by C_v below $T_{\text{low}} \sim 0.5$ K (inset of Fig. 1) is a signature that the system is progressively entering a low-temperature regime characterized by exponentially activated spin excitations over a gap originating from both magnetic dipole-dipole interactions and single-ion anisotropy. We show below via calculations that expand on the authors' previous work, Ref. [55], that the specific heat data of Fig. 1 can be reasonably well described by such gapped magnetic excitations. In other words, we assert that the bulk thermodynamic properties of $\text{Gd}_2\text{Sn}_2\text{O}_7$, revealed by data like that shown in Fig. 1, are compatible with a conventional semi-classical long-range ordered phase. We suggest that specific heat measurements below T_{low} and down to 100 mK could be used to confirm or disprove our proposal. The rest of the paper is organized as follows. We first present a model for exchange and dipole coupled spins on the pyrochlore lattice in the presence of a crystal field inducing single ion spin anisotropy. The Hamiltonian is decoupled via linear spin wave theory, and expressions for the quantum fluctuations and low temperature thermodynamic properties are calculated. We then investigate the effects of second and third nearest neighbor magnetic exchange on the gap to spin wave excitations. Comparing the specific heat calculated in spin wave theory for $\text{Gd}_2\text{Sn}_2\text{O}_7$ to that measured in the experiments of Bonville *et al.*²⁷, we use a maximum likelihood estimator to determine a set of further neighbor couplings which may be present in the material. Finally, we identify the zero temperature quantum fluctuations and present a schematic phase diagram of $\text{Gd}_2\text{Sn}_2\text{O}_7$.

II. MODEL HAMILTONIAN

As reviewed in the previous section, the pyrochlore lattice has evinced much experimental and theoretical interest due to the large degree of geometrical frustration arising from a structure consisting of corner sharing tetrahedra. The cases of $\text{Gd}_2\text{Ti}_2\text{O}_7$ and $\text{Gd}_2\text{Sn}_2\text{O}_7$ are somewhat special, in that the $S = 7/2$ Gd^{3+} S-state ion should

have a relatively small intrinsic anisotropy when compared to other $R_2Ti_2O_7$ pyrochlore oxides. It is known that the titanate ($Gd_2Ti_2O_7$) has a complicated low temperature multi- \mathbf{k} magnetic structure¹⁸. However, recent neutron scattering^{20,27} and electron spin resonance⁵⁴ experiments performed on gadolinium stanate ($Gd_2Sn_2O_7$) indicate that this material exhibits a $\mathbf{k} = 0$ long range ordered state below ~ 1 K. As such, $Gd_2Sn_2O_7$ should be reasonably well described by a general two-body spin interaction Hamiltonian which includes predominant isotropic magnetic exchange interactions up to at least third nearest neighbor and anisotropy in the form of interactions with the local crystal field as well as long range dipole-dipole interactions^{16,20,49,50,51,52}.

Such a Hamiltonian can be written as

$$\mathcal{H} = \mathcal{H}_{\text{ex}} + \mathcal{H}_{\text{dd}} + \mathcal{H}_{\text{cf}}, \quad (1)$$

where the exchange, dipole-dipole and crystal field terms are given by

$$\mathcal{H}_{\text{ex}} = -\frac{1}{2} \sum_{i,a} \sum_{j,b} J_{ab}(\mathbf{R}_{ab}^{ij}) \mathbf{S}_a(\mathbf{R}^i) \cdot \mathbf{S}_b(\mathbf{R}^j) \quad (2a)$$

$$\mathcal{H}_{\text{dd}} = \frac{D_{\text{dd}}}{2} \sum_{i,a} \sum_{j,b} \left\{ \frac{\mathbf{S}_a(\mathbf{R}^i) \cdot \mathbf{S}_b(\mathbf{R}^j)}{|\mathbf{R}_{ab}^{ij}|^3} - 3 \frac{[\mathbf{S}_a(\mathbf{R}^i) \cdot \mathbf{R}_{ab}^{ij}] [\mathbf{S}_b(\mathbf{R}^j) \cdot \mathbf{R}_{ab}^{ij}]}{|\mathbf{R}_{ab}^{ij}|^5} \right\} \quad (2b)$$

$$\mathcal{H}_{\text{cf}} = \sum_{i,a} \sum_{\ell,m} B_{\ell}^m \hat{O}_{\ell}^m [\mathbf{S}_a(\mathbf{R}^i)] \quad (2c)$$

with the factors of 1/2 having been included to avoid double counting. The various conventions used in Eqs. (2a) to (2c) are as follows: $\mathbf{S}_a(\mathbf{R}^i)$ is the spin located on one of N tetrahedra identified by the face centered cubic (FCC) Bravais lattice vector \mathbf{R}^i and the site by one of four tetrahedral sublattice vectors \mathbf{r}_a . $\mathbf{S}_a(\mathbf{R}^i)$ is assumed to be a full $O(3)$ operator satisfying $\mathbf{S}_a(\mathbf{R}^i) \cdot \mathbf{S}_a(\mathbf{R}^i) = S(S+1)$. $J_{ab}(\mathbf{R}_{ab}^{ij})$ gives the value of the isotropic Heisenberg exchange interaction between two spins separated by $\mathbf{R}_{ab}^{ij} = \mathbf{R}^j + \mathbf{r}_b - \mathbf{R}^i - \mathbf{r}_a$, with a negative sign corresponding to antiferromagnetic interactions. In this study, we focus on the $Gd_2Sn_2O_7$ material, and thus consider a fixed value of $J_1 = 3\Theta_{CW}/[zS(S+1)] = -0.273$ K where the Curie-Weiss temperature is $\Theta_{CW} = -8.6$ K and $z = 6$ is the coordination number on the pyrochlore lattice²⁷. We treat the exchange interactions J_2 and J_{31} beyond nearest neighbors as parameters to be adjusted below to produce agreement with experimental (specific heat) measurements on $Gd_2Sn_2O_7$. Following the approach of Wills *et al.*²⁰ we treat the two possible third nearest neighbor (NN) exchange paths J_{31} and J_{32} , known to be present in the pyrochlores^{20,56}, separately (see Fig. 2). With the expectation that $J_{32} \ll J_{31}$, we henceforth set $J_{32} = 0$. The strength of the dipole interaction is given by $D_{\text{dd}} = \mu_0(g\mu_B)^2/4\pi$. At nearest neighbor distance, $R_{\text{nn}} = a\sqrt{2}/4 = 3.695$ Å, where $a = 10.45$ Å is the size

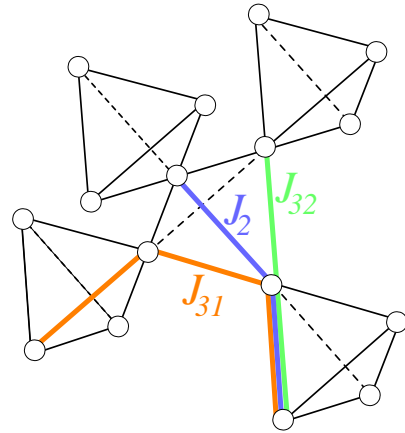


FIG. 2: (Color online) A schematic portion of the pyrochlore lattice, detailing the paths which correspond to second nearest neighbor and two types of third nearest neighbor exchange interactions.

of the cubic unit cell, $D_{\text{dd}}/R_{\text{nn}}^3$ is approximately 15% of the exchange energy J_1 . The crystal field Hamiltonian is written as an expansion of Stevens operators, \hat{O}_{ℓ}^m , that transform like the real tesseral harmonics⁵⁷. The number of terms in the expansion is strongly constrained by symmetry and, from recent electron spin resonance (ESR) measurements⁵⁴, the values of B_2^0 and B_4^0 have been estimated at (47 ± 1) mK and (0.05 ± 0.02) mK, respectively. Here, we only consider the dominant lowest order term in the expansion of \mathcal{H}_{cf} , B_2^0 , which contributes energetically on equal footing with the dipole interactions, and leave the inclusion of higher order corrections to a future study. Writing the Steven's operators in terms of angular momentum operators⁴⁸, the crystal field part of the Hamiltonian \mathcal{H} , \mathcal{H}_{cf} , is:

$$\mathcal{H}_{\text{cf}} = -4NB_2^0S(S+1) + 3B_2^0 \sum_{i,a} [\mathbf{S}_a(\mathbf{R}^i) \cdot \hat{z}_a]^2, \quad (3)$$

where the four unit vectors \hat{z}_a describe the local $\langle 111 \rangle$ direction for each site on a tetrahedron. The conventions and definitions used in this study for all vectors and lengths on the pyrochlore lattice are given in Table 1 of a previous work by one of the authors⁵⁸.

We are interested in the effects of the low energy excitations (spin waves) on the thermodynamic properties of a real material described by Eq. (1). At zero temperature, we assume that the system is in one of the six discrete Palmer-Chalker (PC) $\mathbf{k} = 0$ ground states⁴⁹ depicted in Fig. 3. We have confirmed by direct numerical simulations that the classical zero temperature ground state in a model with nearest-nearest neighbor antiferromagnetic exchange and long-range dipolar interactions at the level of 10 – 20% of the exchange is the PC ground state. See also Refs. [50,51,52]. The use of the PC state for $Gd_2Sn_2O_7$ is supported by recent powder neutron scattering experiments²⁰ where the magnetic diffraction pattern was compared to the expected result from multiple

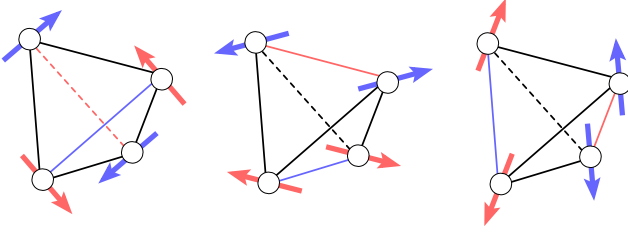


FIG. 3: (Color online) Six degenerate Palmer-Chalker (PC) ground states (reverse spins for other three) for spins on a single tetrahedron. The ground states are characterized by each spin being parallel to an edge of the tetrahedron that does not intersect its vertex and all are tangent to the sphere which circumscribes it. The net magnetic moment on each tetrahedron is identically zero.

candidate ground states. Our approach below will be to analyze the stability of this ground state and its accompanying excitations by investigating the role of quantum fluctuations in reducing the fully polarized classical spin value of $\mathbf{S}_{\text{cl}} = (0, 0, S)$. This can be accomplished by changing the axis of quantization from the global z -direction (an arbitrary choice) to a local axis described by a triad of unit vectors $\{\hat{n}_a^u\}$. This triad is defined such that the locally quantized spin, denoted by a tilde, is related to the spin operator in the Cartesian lab frame via a rotation

$$\begin{aligned} \mathbf{S}_a(\mathbf{R}^i) &= \mathbf{R}(\theta_a, \phi_a) \tilde{\mathbf{S}}_a(\mathbf{R}^i) \\ &= \sum_u \tilde{S}_a^u(\mathbf{R}^i) \hat{n}_a^u \end{aligned} \quad (4)$$

where u runs over the Cartesian indices $\{x, y, z\}$ and \hat{n}_a^z points in the direction of each classical spin. Using Eq. (4) we can rewrite Eq. (1) in a much more compact form

$$\mathcal{H} = -\frac{1}{2} \sum_{a,b} \sum_{i,j} \sum_{u,v} \tilde{S}_a^u(\mathbf{R}^i) \mathcal{J}_{ab}^{uv}(\mathbf{R}_{ab}^{ij}) \tilde{S}_b^v(\mathbf{R}^j), \quad (5)$$

where we have neglected a constant term and

$$\begin{aligned} \mathcal{J}_{ab}^{uv}(\mathbf{R}_{ab}^{ij}) &= J_{ab}(\mathbf{R}_{ab}^{ij}) \hat{n}_a^u \cdot \hat{n}_b^v \\ &- \frac{D_{dd}}{\left| \mathbf{R}_{ab}^{ij} \right|^3} \left[\hat{n}_a^u \cdot \hat{n}_b^v - 3(\hat{n}_a^u \cdot \hat{R}_{ab}^{ij})(\hat{n}_b^v \cdot \hat{R}_{ab}^{ij}) \right] \\ &- 6B_2^0(\hat{n}_a^u \cdot \hat{z}_a)(\hat{n}_b^v \cdot \hat{z}_b) \delta_{a,b} \delta_{u,v}. \end{aligned} \quad (6)$$

Having manipulated our Hamiltonian into a more manageable form, we employ in the next section the methods of linear spin wave theory to diagonalize Eq. (5).

III. LINEAR SPIN WAVE THEORY

In a previous study⁵⁵, which we henceforth refer to as DG, we presented the diagonalization of $\mathcal{H}_{\text{ex}} + \mathcal{H}_{\text{dd}}$

on the pyrochlore lattice via a Holstein-Primakoff⁵⁹ spin wave expansion to order 1/S, through the introduction of bosonic spin deviation (magnon) creation (annihilation) operators c_a^\dagger (c_a). The Ewald summation technique⁶⁰ was used to calculate the Fourier transform of the infinite range dipole-dipole interaction matrix. The calculations of DG can be straightforwardly generalized to include the effects of the crystal field by shifting the diagonal spin interaction matrix elements ($A_{\alpha\alpha}(\mathbf{k})$ and $B_{\alpha\alpha}(\mathbf{k})$) of Eq. (16) in DG by a term proportional to B_2^0 (see Eq. (6)). The result, after the usual Bogoliubov diagonalization procedure, is a Bose gas of non-interacting spin waves described by

$$\mathcal{H} = \mathcal{H}^{(0)} + \sum_{\mathbf{k}} \sum_a \varepsilon_a(\mathbf{k}) \left[a_a^\dagger(\mathbf{k}) a_a(\mathbf{k}) + \frac{1}{2} \right], \quad (7)$$

where the summation is over all wavevectors in the first Brillouin zone (BZ) of the FCC lattice. The dispersion relations for the spin wave modes, $\varepsilon_a(\mathbf{k})$, are calculated from the spectrum of the Bogoliubov transformation. Physically, they are identical to $\varepsilon_a(\mathbf{k}) = \hbar\omega_a(\mathbf{k})$ where $\omega_a(\mathbf{k})$ are the classical excitation frequencies obtained by linearizing the classical equations of motion for interacting magnetic dipoles or rotors⁶¹.

In a real magnet, spin wave fluctuations with dispersion $\varepsilon_a(\mathbf{k})$ raise the classical ground state energy and reduce the staggered magnetic moment per spin from its classical value of S . From Eq. (7), the contribution to the ground state energy is given by

$$\Delta\mathcal{H}^{(0)} = \frac{1}{2} \sum_{\mathbf{k}} \sum_a \varepsilon_a(\mathbf{k}). \quad (8)$$

The full spectrum of the Holstein-Primakoff transformation can be used to calculate the reduction in the staggered magnetization

$$\Delta S = \frac{1}{2} \left(\frac{1}{8N} \sum_{\mathbf{k}} \text{Tr}[\mathbf{Q}^\dagger \mathbf{Q}] - 1 \right), \quad (9)$$

where \mathbf{Q} is the 8×8 hyperbolically normalized matrix of eigenvectors such that $\text{Tr}(\mathbf{Q}^\dagger \mathbf{H} \mathbf{Q}) = \sum_a \varepsilon_a(\mathbf{k})$ and \mathbf{H} is the 8×8 block matrix Hamiltonian [see DG Eqs. (16) and (19)]. N is the number of tetrahedra on a pyrochlore lattice with periodic boundary conditions.

At low temperatures ($k_B T < \varepsilon_a(\mathbf{k})$) expressions for the specific heat at constant volume, C_v , and staggered magnetization, $m = S - \Delta S$, can be derived from the classical partition function $\mathcal{Z} = \text{Tr}[\exp(-\beta\mathcal{H})]$ corresponding to Eq. (7). Using Eqs. (7) to (9), we find (see DG)

$$C_v = \beta^2 \sum_{\mathbf{k}} \sum_a [\varepsilon_a(\mathbf{k}) n_B(\varepsilon_a(\mathbf{k}))]^2 \exp[\beta\varepsilon_a(\mathbf{k})], \quad (10)$$

$$\begin{aligned} m &= S + \frac{1}{2} \\ &- \frac{1}{8N} \sum_{\mathbf{k}} \sum_a [\mathbf{Q}^\dagger \mathbf{Q}]_{aa} [1 + n_B(\varepsilon_a(\mathbf{k}))], \end{aligned} \quad (11)$$

where β is the inverse temperature and $n_B(\varepsilon_a(\mathbf{k})) = 1/(e^{\beta\varepsilon_a(\mathbf{k})} - 1)$ is the Bose distribution function.

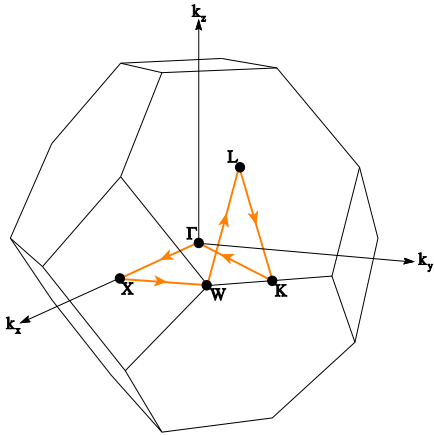


FIG. 4: (Color online) The first Brillouin zone of the pyrochlore lattice, showing the five high symmetry points $\Gamma = (0, 0, 0)$, $X = 2\pi/a(1, 0, 0)$, $W = 2\pi/a(1, 1/2, 0)$, $L = 2\pi/a(1/2, 1/2, 1/2)$ and $K = 2\pi/a(3/4, 3/4, 0)$ and the path in k -space along which spectra are plotted in this study.

IV. RESULTS

Having determined the expressions for the zero temperature quantum fluctuations, as well as finite temperature thermodynamic relations of a dipolar Heisenberg model with crystal field interactions on the pyrochlore lattice, we may now study the quantitative effects of perturbative J_2 and J_{31} for fixed J_1 and B_2^0 . The limit of stability of the proposed PC classical ground states on the pyrochlore lattice can be investigated by searching for soft modes ($\varepsilon_a(\mathbf{k}) \rightarrow 0$) at some wavevector \mathbf{k} .

A. Second and third NN exchange

If we ignore all interactions except nearest neighbor isotropic antiferromagnetic exchange, it has been known for some time⁶² that both classical² and quantum⁵ spins on the pyrochlore lattice fail to develop conventional long range magnetic order at nonzero temperature. There exists two unbroken symmetries in the ground state manifold^{1,3} corresponding to lattice translation and time reversal. The excitation spectrum consists of two sets of two degenerate modes, the first being soft over the entire Brillouin zone, (see Fig. 4) and the second are acoustic and linear along $\Gamma \rightarrow X$ leading to divergent quantum fluctuations. The inclusion of both dipole-dipole, and crystal field interactions break the rotational symmetry and lift *all* excitations to finite frequency⁵⁵.

Fig. 5 shows the dispersion spectrum of the four spin wave modes for three values of J_2 and J_{31} along the high symmetry path described in Fig. 4. We do indeed observe only optical modes, with degeneracy preserved along $X \rightarrow W$ for $J_2 = J_{31} = 0$. The qualitative behavior of $\varepsilon_a(\mathbf{k})$ with varying J_2 and J_{31} also seems to confirm the naive expectation that even perturbatively

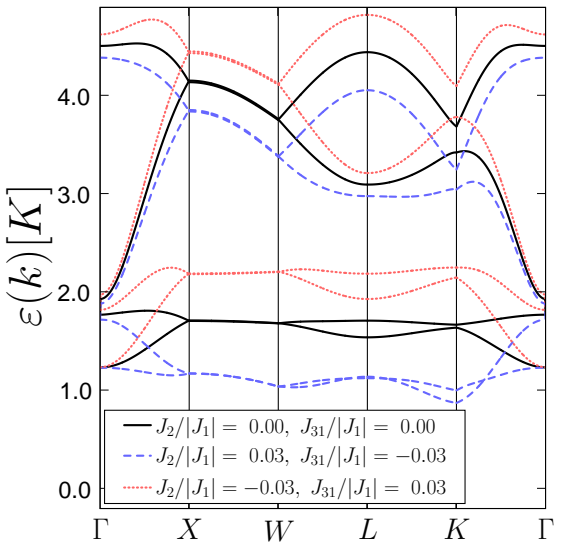


FIG. 5: (Color online) The spin wave excitation spectrum in kelvin for $(J_2/|J_1|, J_{31}/|J_1|)$ equal to $(0.0, 0.0)$, $(0.03, -0.03)$ and $(-0.03, 0.03)$ plotted along a high-symmetry path in the first Brillouin zone of the FCC lattice. For the three parameter sets shown there exists a finite gap to spin wave excitations throughout the zone.

small third nearest antiferromagnetic neighbor exchange should reduce the stability of the PC states^{20,50,51}. It also appears that the minimum excitation gap does not always occur at $\mathbf{k} = 0$ indicating the underlying presence of a finite wavevector instability as J_2 and J_{31} are tuned away from $J_2 = J_{31} = 0$.

The spin wave energy gap can be analyzed more quantitatively by defining

$$\Delta(\mathbf{k}) \equiv \min_a [\varepsilon_a(\mathbf{k})] \quad (12a)$$

$$\Delta \equiv \min_{\mathbf{k}} [\Delta(\mathbf{k})]. \quad (12b)$$

The value of $\Delta(\mathbf{k})$ can be investigated as a function of J_2 and J_{31} at each of the high symmetry points described above. As we vary J_2 and J_{31} through some critical values, instabilities first appear at these wavevectors of high symmetry. The resulting gap values are shown in Fig. 6. Although $\Delta(\Gamma) > 0$ for all values of J_2 and J_{31} studied here, the region of stability of the PC states is defined by the observed appearance of soft modes, at $\mathbf{k} = K = 2\pi/a(3/4, 3/4, 0)$ for ferromagnetic (positive) J_2 and antiferromagnetic (negative) J_{31} . Performing a search for the minimum value of the gap over the entire Brillouin zone (Δ) at each value of J_2 and J_{31} confirms that the instability first appears at the K -point. The effect of perturbative second and third NN exchange interactions on the global minimum energy gap (Eq. (12b)) along with the corresponding magnitude of spin fluctuations $\Delta S/S$ (Eq. (9)) is shown in Fig. 7. Here we observe that upon reaching a pair of critical values for $|J_2/|J_1|$ and $|J_{31}/|J_1|$, the excitation gap is suppressed to zero

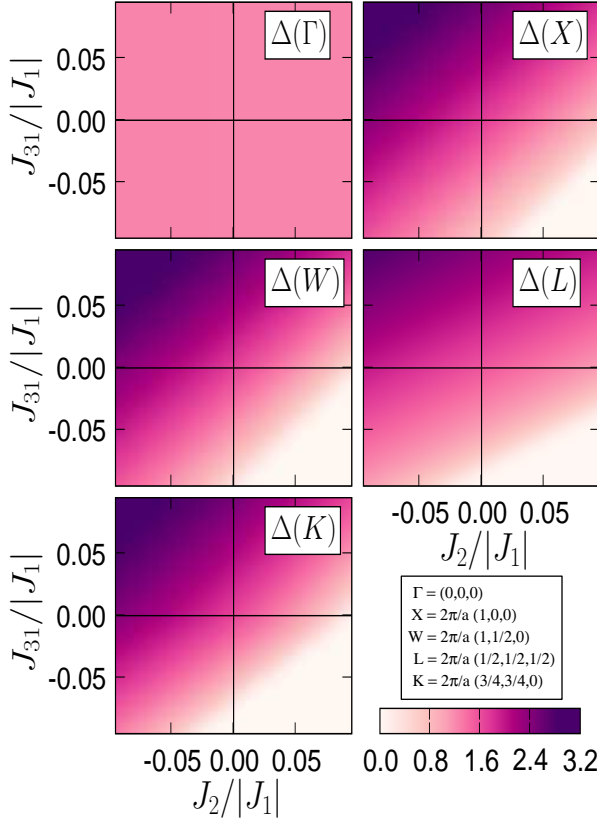


FIG. 6: (Color online) The magnitude of the lowest spin wave excitation energy $\Delta(k)$ in kelvin at various high symmetry points in the first BZ plotted in the $J_2 - J_{31}$ plane. All panels are plotted with the same color scale making the slight variations in the gap at $\Gamma = (0, 0, 0)$ difficult to discern. A soft mode instability occurs only for antiferromagnetic third NN coupling J_{31}

(top panel), and divergent spin fluctuations ensue (bottom panel). The values of J_2 and J_{31} corresponding to $\Delta \rightarrow 0$ can be identified, and are best described by the linear relationship $J_{31} = 0.750J_2 - 0.077|J_1|$. This line defines the phase boundary between a sector of stability for the $\mathbf{k} = 0$ PC ground states, and a region characterized by instabilities at finite wavevector. In addition, this line corresponds to the white regions in Fig. 6 where $\Delta \rightarrow 0$, and thus defines the limit of applicability of the spin wave calculation around the PC ground state described in Section III.

Plotting $\Delta(\mathbf{k})$ along $\Gamma \rightarrow X \rightarrow W \rightarrow L \rightarrow K \rightarrow \Gamma$ with J_{31} pinned to this phase boundary leads to the spectrum shown in Fig. 8. It is apparent from this result, that once the value of the third NN exchange constant has been set at a suitably antiferromagnetic value, altering the second NN exchange constant, has a relatively limited effect on the gap and on the consequential proliferation of quantum fluctuations about the classical ground state.

To summarize, the effects of perturbative second and third NN exchange interactions on the appearance of soft

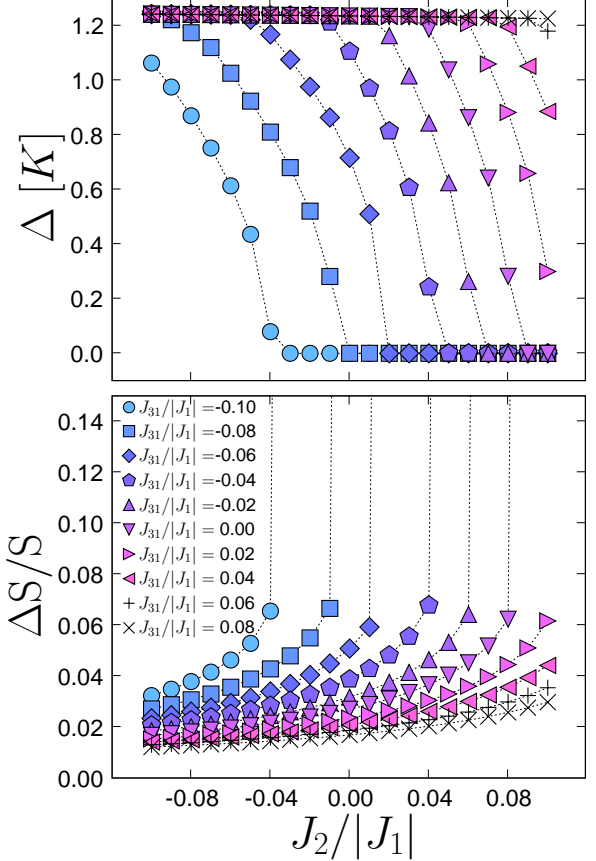


FIG. 7: (Color online) The spin wave excitation gap in kelvin (Δ , top panel) found by determining the minimum energy over 19^3 discrete points in the first BZ, and the reduction in sublattice magnetization ($\Delta S/S$, bottom panel) for various values of $J_{31}/|J_1|$ plotted against $J_2/|J_1|$. The jump in $\Delta S/S$ occurs once the limit of stability of the $\mathbf{k} = 0$ Palmer-Chalker ground state is reached. Both panels share a common legend.

modes and their accompanying quantum fluctuations in a model of a dipolar coupled antiferromagnetic Heisenberg pyrochlore with single-ion anisotropy is globally illustrated in Figs. 5-8. Such a model should well characterize the low temperature behavior of $\text{Gd}_2\text{Sn}_2\text{O}_7$, and we next apply these tools with the goal of searching for the unconventional spin excitations believed to be present in this material on the basis of the unconventional $C_v \propto T^2$ specific heat in the temperature range [350, 800] mK.

B. The case of $\text{Gd}_2\text{Sn}_2\text{O}_7$

As described in the Introduction, recent studies^{27,53} of $\text{Gd}_2\text{Sn}_2\text{O}_7$ have reported, on the basis of μSR measurements, evidence for Gd^{3+} spin dynamics well below 0.9 K, as well as suggesting that the low temperature specific heat is accurately described by an anomalous T^2 power law. This is in stark contrast with the expected T^3

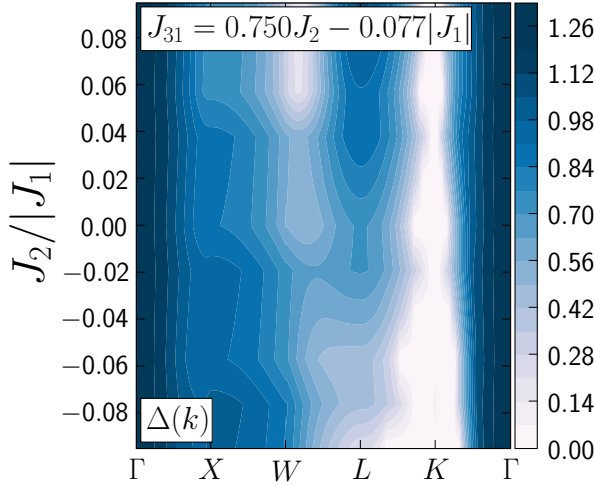


FIG. 8: (Color online) The lowest excitation energy $\Delta(k)$ in kelvin plotted along the high symmetry path discussed in the text with (J_2, J_{31}) fixed to reside on the phase boundary parameterized by $J_{31} = 0.750J_2 - 0.077$. The location of the zero modes in k -space indicate that the instability out of the PC states occurs via excitations described by $\mathbf{k} = 2\pi/a(3/4, 3/4, 0)$.

behavior for a three dimensional antiferromagnet, with possible exponential suppression at a temperature below a characteristic excitation gap.

On the other hand, the long-range ordered state found by neutron scattering in $\text{Gd}_2\text{Sn}_2\text{O}_7$ is that predicted by the simple model of Eq. 1 in Section III and discussed in Refs. [16,49,50,51,52] and, consequently, the low-temperature behavior of this material should be well described by linear spin wave theory. Thus, in an attempt to resolve the paradox offered by the $C_v \sim T^2$ behavior, we have calculated the low temperature specific heat via Eq (10) within the $J_2 - J_{31}$ plane, and have performed a search for the parameters which best reproduce the reported low temperature specific heat²⁷. This was accomplished by performing least squares linear fits of $\log C_v$ vs $1/T$ for $T < 0.5$ K between the experimental data and the spin wave specific heat for approximately 500 values of J_2 and J_{31} . A characteristic subset of the large number of performed fits are displayed in Fig. 9. The values of J_2 and J_{31} which provided the best fit to the experimental data can be quantified by defining a maximum likelihood estimator χ^2 which is shown in Fig. 10. It is important to note that the fits of the specific heat, C_v , discussed here, were done with an *absolute* dimensionfull scale, and thus no vertical adjustment of the experimental data was allowed. The comparisons allow only for adjustments of J_2 and J_{31} which are therefore *fine-tuning* effects. As such, it appears that a model which possesses solely nearest-neighbor exchange, long-range dipolar interactions and single-ion anisotropy *already* leads to a reasonable semi-quantitative description of the C_v data below 500 mK. This indicates that the temperature $T \sim 500$ mK corre-

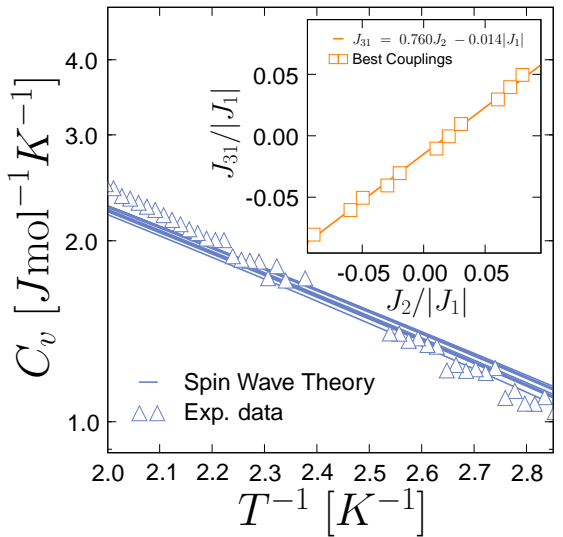


FIG. 9: (Color online) The low temperature specific heat from Ref. [27] plotted against inverse temperature on a logarithmic scale. The lines are the calculated value of the specific heat using the ten best fit values for $(J_2/|J_1|, J_{31}/|J_1|)$ (as seen in the inset).

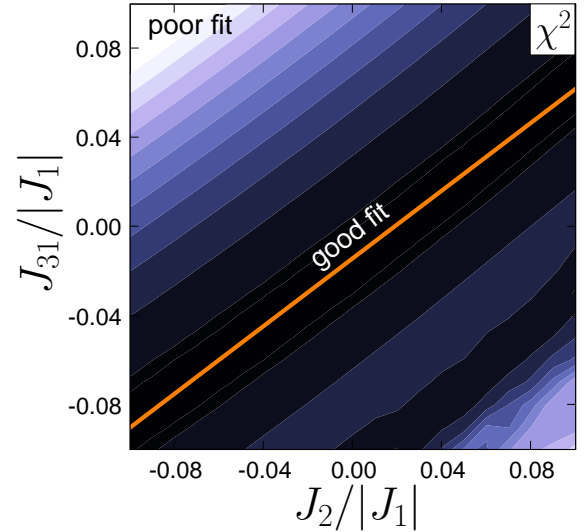


FIG. 10: (Color online) The value of the maximum likelihood estimator (χ^2) in the $J_2 - J_{31}$ plane for a fit of the logarithm of the specific heat at low temperatures ($T < 0.5$ K) calculated using linear spin wave theory and compared with the experimental data of Ref. [27]. The parameters $(J_2/|J_1|, J_{31}/|J_1|)$ with the smallest χ^2 , giving the most effective fit, fall along the indicated line $J_{31} = 0.760J_2 - 0.014|J_1|$.

sponds to the upper temperature below which magnetic excitations become thermally activated.

The minimum of χ^2 in the $J_2 - J_{31}$ plane falls along the straight line $J_{31} = 0.760J_2 - 0.014|J_1|$. This line of best fit also falls in a region of large stability (highly gapped spin wave excitations) for the classical PC ground states

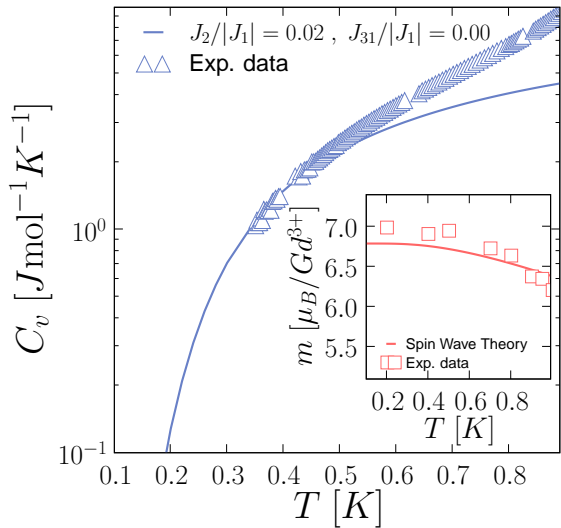


FIG. 11: (Color online) The low temperature specific heat (data from Ref. [27]) versus temperature on a logarithmic scale. The calculated specific heat is plotted for the parameter set $J_2 = 0.02$, $J_{31} = 0.0$ which had the smallest χ^2 , although any values close to the line mentioned in the text give a qualitatively very similar result. The agreement is quite good at low temperatures, where spin wave theory should be applicable. The low temperature suppression of C_v is characteristic of gapped excitations, in contrast with previously reported power law behavior^{27,53}. The inset displays the temperature dependence of the Gd^{3+} moment calculated using a Bose gas of excitations along with the value measured from ¹⁵⁵Gd Mössbauer measurements²⁷.

with respect to quantum fluctuations (see Fig. 6).

The poorness of fit for simultaneously strong ferromagnetic second NN and antiferromagnetic third NN interactions or vice versa (top left, or lower right of Fig. 10), seems to indicate that is quite unlikely that $\text{Gd}_2\text{Sn}_2\text{O}_7$ resides in these portions of the phase diagram. The parameters $J_2 = 0.02$ and $J_{31} = 0.0$ provide the *best* empirical fit to the experimental specific heat data, although qualitatively similar fits are seen for all parameters which satisfy $J_{31} = 0.760J_2 - 0.014|J_1|$. Setting the parameters to these particular values, we display the spin wave specific heat, as well as the temperature dependence of the order parameter m in Fig. 11. Again, as shown in Fig. 9, it is clear that at low temperatures, ($T \leq 370$ mK), the experimental specific heat data systematically falls below the gapped spin wave results. This behavior is tentatively consistent with the fact that spin wave theory produces a smaller value for the magnetization m than what is measured from Mössbauer experiments. However, we note that due to the intrinsic short dynamical time scale probed by Mössbauer measurements, the experimental data in the inset of Fig. 11 may not reflect the true value of the infinite-time order parameter.

It is perhaps worthwhile to make a few comments on the physical meaning of the above fits. Firstly, we note that because of the weakly dispersive nature of the two

lowest lying gapped magnon excitations (see Fig. 5), the temperature dependence of thermodynamics quantities in the pyrochlore Heisenberg antiferromagnet plus dipolar interactions do not display the typical $C_v \sim T^3$ behavior as the temperature reaches approximately 0.5 K and exits its characteristic low-temperature exponential behavior. In fact, such an observation was already made in Ref. [55] independently of any attempt to describe C_v for $\text{Gd}_2\text{Sn}_2\text{O}_7$. Secondly, the calculations presented here constitute a standard procedure for a system with conventional long range magnetic order. In this context, it is therefore interesting to note that, contrary to the reported T^2 behavior, the experimental specific heat data are not only relatively well fit using the exponential spin wave form of Eq. (10), but it appears to fall off even faster than the exponentials considered at low temperatures. This would lend credence to the view that analyzing experimental data on a log-log scale over a limited range, can lead to specious power law fits. Hence, and on the basis of specific heat measurements *alone* (i.e. without consideration of the $1/T_1$ μ SR spin-lattice relaxation rate), it would therefore appear that the suggestion of unconventional excitations in $\text{Gd}_2\text{Sn}_2\text{O}_7$ should be challenged by the principle of “Ockham’s razor”. We are therefore led to suggest that the description of the specific heat C_v in terms of an anomalous power law, $C_v \sim T^2$, in a *reduced* and *intermediate* temperature range $T \in [350, 800]$ mK does not provide a convincing indicator for anomalous excitations out of the ground state of $\text{Gd}_2\text{Sn}_2\text{O}_7$. Unlike the suggestion made in Ref. [53] on the basis of the temperature independence of the $1/T_1$ muon spin relaxation rate below $T_c \sim 1$ K, we have found a fully gapped spin wave spectrum with no density of states at zero energy. Hence, at this time, the microscopic origin of the temperature independence of $1/T_1$ found below T_c in $\text{Gd}_2\text{Sn}_2\text{O}_7$ remains to be understood.

C. Ground state properties

In the previous section, we have identified a relationship between the second J_2 and third J_{31} NN exchange constants which best reproduce the low temperature thermodynamic behavior in $\text{Gd}_2\text{Sn}_2\text{O}_7$. We now investigate the role of quantum fluctuations. Fig. 12 displays both the minimum spin wave energy gap Δ and the reduction in the staggered moment $\Delta S/S$ along the line of best fit $J_{31} = 0.760J_2 - 0.014|J_1|$. This result details the complicated relationship between the value of the gap, and the stability of the ground state, i.e. a decrease in the global spin wave energy gap (which may only occur at a single \mathbf{k} -point) does not immediately trigger an increase of moderate quantum fluctuations. Indeed, the opposite behavior is seen in Fig. 12. In an exchange coupled Heisenberg antiferromagnet on a non-Bravais lattice, the specifics of all relative energy scales come into play, and one must not neglect the effects of weakly dispersing optical modes. All the results presented here can be

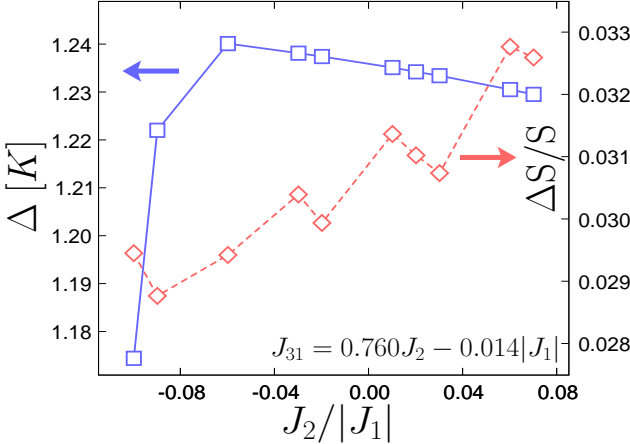


FIG. 12: (Color online) The global spin wave energy gap (left scale) and the reduction in the staggered moment (right scale) along the line in the $J_2 - J_{31}$ plane most closely corresponding to the parameter set of $\text{Gd}_2\text{Sn}_2\text{O}_7$.

compiled into an effective schematic phase diagram for $\text{Gd}_2\text{Sn}_2\text{O}_7$. Fig. 13 depicts the separatrix in the $J_2 - J_{31}$ plane (solid line) that delineates the limit of stability of the $k = 0$ PC state against a soft mode characterized by wavevector $2\pi/a(3/4, 3/4, 0)$, i.e. the K -point. Possibly relevant values of J_2 and J_{31} for which χ^2 reaches its minimum value are shown as the parametric dashed line $J_{31} = 0.760J_2 - 0.014|J_1|$. We note that Fig. 13 shows a zero temperature phase diagram that delineates the limit of stability of the $k = 0$ Palmer-Chalker ground state against an instability at $2\pi/a(3/4, 3/4, 0)$. A similar phase diagram presented in Ref. [20] (with the signs corresponding to FM and AF interactions reversed) gives the ordering wave vector of the long range magnetic ordered state that first develops as the system is cooled down from the paramagnetic phase.

V. DISCUSSION

We have considered a Heisenberg model that includes isotropic exchange interactions up to third nearest-neighbors, single-ion anisotropy and long-range magnetic dipole-dipole interactions to describe the long-range ordered state of the $\text{Gd}_2\text{Sn}_2\text{O}_7$ pyrochlore antiferromagnet. The ground state of this system, as found by neutron scattering experiments, corresponds to the (classical, PC) ground state described by Palmer and Chalker⁴⁹ for the classical Heisenberg pyrochlore with nearest-neighbor antiferromagnetic exchange and long-range dipolar couplings^{16,51,52}. We used a long wavelength (1/S spin wave) expansion to describe the low-energy excitations about the PC ground state and to calculate the low-temperature behavior of the specific heat, C_v , and order parameter, m , for this material.

By fitting the available specific heat data in the low-

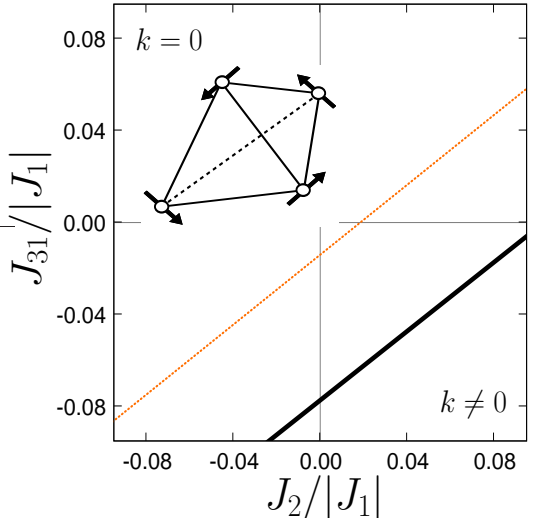


FIG. 13: (Color online) The $J_2 - J_{31}$ ground state phase diagram showing regions with order characterized by zero and non-zero wavevectors. The solid black line delineates the limit of stability of the Palmer-Chalker ground state. The inset tetrahedron is tiled with one of the PC states, and the dashed line $J_{31} = 0.760J_2 - 0.014|J_1|$ corresponds to the values of J_2 and J_{31} which produced the best fits to experimental data.

temperature range ($0.35 \text{ K} < T < 0.5 \text{ K}$), we were able to procure an estimate of the exchange interactions beyond nearest neighbors. We obtained evidence that $\text{Gd}_2\text{Sn}_2\text{O}_7$ is in a region of exchange coupling with large stability against quantum fluctuations. Our main result (which *does not* rely on excruciatingly fine-tuned exchange constants beyond nearest-neighbor) is that the experimental temperature range $0.35 \text{ K} < T < 0.5 \text{ K}$ corresponds to the upper temperature range below which the thermodynamic quantities become thermally activated above an excitation gap $\Delta \sim 1 \text{ K}^{55}$. In other words, the independently experimentally determined microscopic nearest-neighbor exchange (on the basis of DC magnetic susceptibility), single-ion anisotropy (on the basis of ESR) and dipolar coupling strength already predict a temperature dependence for C_v in $\text{Gd}_2\text{Sn}_2\text{O}_7$ that is in rough agreement with the experiment without significant adjustment.

The excitation gap takes its origin from the combination of single-ion anisotropy and magnetic dipolar anisotropy. From our fits of the experimental specific heat, we tentatively conclude that the real gap is actually even *larger* than the one we have determined. Specifically, considering the lower temperature range in Fig. 9 and Fig. 11 (and the inset of Fig. 11 for m), it appears that the specific heat is dropping faster in the lower temperature range than the calculations predict. We speculate that this may indicate that the sub-leading anisotropy terms neglected in \mathcal{H}_{cf} in Eq. (5) (and which correspond to crystal field terms $B_{l,m}$ with $l = 4, 6$) would further increase the effective gap. In particular,

those corrections would resign to further limit the spin fluctuations perpendicular to the local three-fold axis. However, at this time, experimental measurements of C_v below 0.3 K are required to ascertain quantitatively the detail of the microscopic parameters for $\text{Gd}_2\text{Sn}_2\text{O}_7$ and to determine with better precision the exchange parameters J_1 , J_2 and J_{31} . As in other Gd^{3+} -based insulating magnetic materials^{63,64}, it is also possible that anisotropic exchange interactions ultimately need to be included in a complete description of $\text{Gd}_2\text{Sn}_2\text{O}_7$.

It therefore appears that a rejoinder to the question posed in the Introduction is that the low temperature specific heat observed in gadolinium stanate ($\text{Gd}_2\text{Sn}_2\text{O}_7$) may possibly be well described by the conventional gapped spin wave excitations of Ref. [55]. We believe that either a confirmation or rebuttal of our suggestion of gapped excitations in $\text{Gd}_2\text{Sn}_2\text{O}_7$ via specific heat (C_v) measurements down to ~ 100 mK would tremendously help focus the discussion about the pervasive low energy excitations in insulating magnetic rare-earth pyrochlore oxides. However, a possible confirmation of such gapped excitations in $\text{Gd}_2\text{Sn}_2\text{O}_7$ via specific heat measurements would ultimately have to be rational-

ized within the context of the perplexing and persistent temperature-independent spin dynamics found in muon spin relaxation studies on this, and other geometrically frustrated pyrochlores.

VI. ACKNOWLEDGMENTS

We are indebted to Pierre Bonville for kindly providing us with the low temperature specific heat and Mössbauer data used for all the fits reported in this study. We thank Matt Enjalran, Tom Fennell and Mike Zhitomirsky for useful and stimulating discussions. Support for this work was provided by the NSERC of Canada and the Canada Research Chair Program (Tier I) (M.G), the NSERC of Canada Grant PGS D2-316308-2005 (A.D.), the Canada Foundation for Innovation, the Ontario Innovation Trust, and the Canadian Institute for Advanced research. M.G. acknowledges the University of Canterbury for an Erskine Fellowship and the hospitality of the Department of Physics and Astronomy at the University of Canterbury where part of this work was completed.

¹ J. N. Reimers, A. J. Berlinsky, and A.-C. Shi, Phys. Rev. B **43**, 865 (1992).

² R. Moessner and J. T. Chalker, Phys. Rev. Lett. **80**, 2929 (1998).

³ R. Moessner, Can. J. Phys. **79**, 1283 (2001).

⁴ R. Moessner and J. T. Chalker, Phys. Rev. B **58**, 12049 (1998).

⁵ B. Canals and C. Lacroix, Phys. Rev. Lett. **80**, 2933 (1998).

⁶ J. E. Greedan, Journal of Materials Chemistry **11**, 37 (2001).

⁷ J. E. Greedan, M. Sato, X. U. Yan, and F. S. Razavi, Solid State Comm. **59**, 895 (1986).

⁸ M. J. P. Gingras, C. V. Stager, N. P. Raju, B. D. Gaulin, and J. E. Greedan, Phys. Rev. Lett. **78**, 947 (1997).

⁹ J. S. Gardner, B. D. Gaulin, S. H. Lee, C. Broholm, N. P. Raju, and J. E. Greedan, Phys. Rev. Lett. **83**, 211 (1999).

¹⁰ A. Keren and J. S. Gardner, Phys. Rev. Lett. **87**, 177201 (2001).

¹¹ B. D. Gaulin, J. N. Reimers, T. E. Mason, J. E. Greedan, and Z. Tun, Phys. Rev. Lett. **69**, 3244 (1992).

¹² M. J. Harris, S. T. Bramwell, D. F. McMorrow, T. Zeiske, and K. W. Godfrey, Phys. Rev. Lett. **79**, 2554 (1997).

¹³ S. T. Bramwell, M. J. Harris, B. C. den Hertog, M. J. P. Gingras, J. S. Gardner, D. F. McMorrow, A. R. Wildes, A. L. Cornelius, J. D. M. Champion, R. G. Melko, et al., Phys. Rev. Lett. **87**, 47205 (2001).

¹⁴ A. L. Cornelius and J. S. Gardner, Phys. Rev. B **64**, 60406 (2001).

¹⁵ A. P. Ramirez, A. Hayashi, R. J. Cava, R. Siddharthan, and B. S. Shastry, Nature **399**, 333 (1999).

¹⁶ N. P. Raju, M. Dion, M. J. P. Gingras, T. E. Mason, and J. E. Greedan, Phys. Rev. B **59**, 14489 (1999).

¹⁷ A. P. Ramirez, B. S. Shastry, A. Hayashi, J. J. Krajewski, D. A. Huse, and R. J. Cava, Phys. Rev. Lett. **89**, 67202 (2002).

¹⁸ J. R. Stewart, G. Ehlers, A. S. Wills, S. T. Bramwell, and J. S. Gardner, J. Phys.: Condens. Matter **16**, L321 (2004).

¹⁹ J. D. M. Champion, M. J. Harris, P. C. W. Holdsworth, A. S. Wills, G. Balakrishnan, S. T. Bramwell, E. Čížmár, T. Fennell, J. S. Gardner, J. Lago, et al., Phys. Rev. B **68**, 020401 (2003).

²⁰ A. S. Wills, M. E. Zhitomirsky, B. Canals, J. P. Sanchez, P. Bonville, P. Dalmas de Réotier, and A. Yaouanc, J. Phys.: Condens. Matter **18** (2006).

²¹ J. S. Gardner, S. R. Dunsiger, B. D. Gaulin, M. J. P. Gingras, J. E. Greedan, R. F. Kiefl, M. D. Lumsden, W. A. MacFarlane, N. P. Raju, J. E. Sonier, et al., Phys. Rev. Lett. **82**, 1012 (1999).

²² J. S. Gardner, A. Keren, G. Ehlers, C. Stock, E. Segal, J. M. Roper, B. Fåk, M. B. Stone, P. R. Hammar, D. H. Reich, et al., Phys. Rev. B **68**, 180401 (2003).

²³ Y.-J. Kao, M. Enjalran, A. G. Del Maestro, H. R. Molavian, and M. J. P. Gingras, Phys. Rev. B **68**, 172407 (2003).

²⁴ M. Enjalran, M. J. P. Gingras, Y. J. Kao, A. G. Del Maestro, and H. R. Molavian, J. Phys.: Condens. Matter **16**, S673 (2004).

²⁵ I. Mirebeau, A. Apetrei, I. N. Goncharenko, and R. Moessner, Physica B: Condensed Matter **385-386**, 307 (2006).

²⁶ H. R. Molavian, M. J. P. Gingras, and B. Canals, Phys. Rev. Lett. p. 157204 (2007).

²⁷ P. Bonville, J. A. Hodges, M. Ocio, J. P. Sanchez, P. Vuliet, S. Sosin, and D. Braithwaite, J. Physics: Condens. Matter **15**, 7777 (2003).

²⁸ J. S. Gardner, G. Ehlers, S. T. Bramwell, and B. D. Gaulin, J. Phys.: Condens. Matter **16**, S643 (2004).

²⁹ J. A. Hodges, P. Bonville, A. Forget, A. Yaouanc, P. Dal-

mas de Réotier, G. André, M. Rams, K. Królas, C. Ritter, P. C. M. Gubbens, et al., *Phys. Rev. Lett.* **88**, 77204 (2002).

³⁰ S. R. Dunsiger, J. S. Gardner, J. A. Chakhalian, A. L. Cornelius, M. Jaime, R. F. Kiefl, R. Movshovich, W. A. MacFarlane, R. I. Miller, J. E. Sonier, et al., *Phys. Rev. Lett.* **85**, 3504 (2000).

³¹ I. M. Marshall, S. J. Blundell, F. L. Pratt, A. Husmann, C. A. Steer, A. I. Coldea, W. Hayes, and R. C. C. Ward, *J. Phys.: Condens. Matter* **14**, L157 (2002).

³² Y. J. Uemura, A. Keren, K. Kojima, L. P. Le, G. M. Luke, W. D. Wu, Y. Ajiro, T. Asano, Y. Kuriyama, M. Mekata, et al., *Phys. Rev. Lett.* **73**, 3306 (1994).

³³ P. Bonville, J. A. Hodges, E. Bertin, J. P. Bouchaud, M. Ocio, et al., *cond-mat/0306470* (2003).

³⁴ L. Pauling, *Journal of the American Chemical Society* **57**, 2680 (1935).

³⁵ W. F. Giauque and J. W. Stout, *Journal of the American Chemical Society* **58**, 1144 (1936).

³⁶ S. T. Bramwell and M. J. P. Gingras, *Science* **294**, 1495 (2001).

³⁷ B. C. den Hertog and M. J. P. Gingras, *Phys. Rev. Lett.* **84**, 3430 (2000).

³⁸ R. G. Melko and M. J. P. Gingras, *J. Phys.: Condens. Matter* **16**, R1277 (2004).

³⁹ H. Fukazawa, R. G. Melko, R. Higashinaka, Y. Maeno, and M. J. P. Gingras, *Phys. Rev. B* **65**, 054410 (2002).

⁴⁰ M. J. Harris, S. T. Bramwell, T. Zeiske, D. F. McMorrow, and P. J. C. King, *J. of Mag. and Magn. Mater.* **177**, 757 (1998).

⁴¹ G. Ehlers, A. L. Cornelius, T. Fennell, M. Koza, S. T. Bramwell, and J. S. Gardner, *J. Phys.: Condens. Matter* **16**, S635 (2004).

⁴² I. Mirebeau, A. Apetrei, J. Rodríguez-Carvajal, P. Bonville, A. Forget, D. Colson, V. Glazkov, J. P. Sanchez, O. Isnard, and E. Suard, *Phys. Rev. Lett.* **94**, 246402 (2005).

⁴³ P. Dalmas de Réotier, A. Yaouanc, L. Keller, A. Cervellino, B. Roessli, C. Baines, A. Forget, C. Vaju, P. Gubbens, A. Amato, et al., *Phys Rev Lett* **96**, 127202 (2006).

⁴⁴ F. Bert, P. Mendels, A. Olariu, N. Blanchard, G. Collin, A. Amato, C. Baines, and A. D. Hillier, *Phys. Rev. Lett.* **97**, 117203 (2006).

⁴⁵ J. Lago, T. Lancaster, S. J. Blundell, S. T. Bramwell, F. L. Pratt, M. Shirai, and C. Baines, *Journal of Physics: Condensed Matter* **17**, 979 (2005).

⁴⁶ A. Yaouanc, P. Dalmas de Réotier, V. Glazkov, C. Marin, P. Bonville, J. A. Hodges, P. C. M. Gubbens, S. Sakarya, and C. Baines, *Phys. Rev. Lett.* **95**, 047203 (2005).

⁴⁷ S. R. Dunsiger, R. F. Kiefl, J. A. Chakhalian, J. E. Greedan, W. A. MacFarlane, R. I. Miller, G. D. Morris, A. N. Price, N. P. Raju, and J. E. Sonier, *Phys. Rev. B* **73**, 172418 (2006).

⁴⁸ J. Jensen and A. Makintosh, *Rare Earth Magnetism* (Clarendon Press, Oxford, 1991).

⁴⁹ S. E. Palmer and J. T. Chalker, *Phys. Rev. B* **62**, 488 (2000).

⁵⁰ M. Enjalran and M. J. P. Gingras, *cond-mat/0307152* (2003).

⁵¹ O. Cépas and B. S. Shastry, *Phys. Rev. B* **69**, 184402 (2004).

⁵² O. Cépas, B. S. Shastry, and A. P. Young, *Phys. Rev. B* **72**, 184408 (2005).

⁵³ P. Bonville, J. A. Hodges, E. Bertin, J. P. Bouchaud, P. Dalmas De Réotier, L. P. Regnault, H. M. Rønnow, J. P. Sanches, S. Sosin, and A. Yaouanc, *Hyperfine Interactions* **156/157**, 103 (2004).

⁵⁴ V. N. Glazkov, A. I. Smirnov, J. P. Sanchez, A. Forget, D. Colson, and P. Bonville, *J. Phys.: Condens. Matter* **18**, 2285 (2006).

⁵⁵ A. G. Del Maestro and M. J. P. Gingras, *J. Phys.: Condens. Matter* **16**, 3339 (2004).

⁵⁶ B. J. Kennedy, B. A. Hunter, and C. J. Howard, *Journal of Solid State Chemistry* **130**, 58 (1997).

⁵⁷ M. T. Hutchings, in *Solid State Physics*, edited by F. Seitz, D. Turnbull, and H. Ehrenreich (Academic Press, New York, 1964), vol. 16, p. 227.

⁵⁸ M. Enjalran and M. J. P. Gingras, *Phys. Rev. B* **70**, 174426 (2004).

⁵⁹ T. Holstein and H. Primakoff, *Phys. Rev.* **58**, 1098 (1940).

⁶⁰ P. P. Ewald, *Ann. Physick* **64**, 253 (1921).

⁶¹ A. Del Maestro, Master's thesis, University of Waterloo (2003).

⁶² J. Villain, *Zeitschrift für Physik B Condensed Matter* **33**, 31 (1979).

⁶³ R. S. Meltzer and R. L. Cone, *Phys. Rev. B* **13**, 2818 (1976).

⁶⁴ R. L. Cone and R. S. Meltzer, *Phys. Rev. Lett.* **30**, 859 (1973).